

# Electrodeposition of selenium, indium and copper in an air- and water-stable ionic liquid at variable temperatures

S. Zein El Abedin<sup>1</sup>, A.Y. Saad<sup>1</sup>, H.K. Farag<sup>2</sup>, N. Borisenko, Q.X. Liu, F. Endres\*

*Faculty of Natural and Materials Sciences, Clausthal University of Technology, Robert-Koch-Str. 42, D-38678 Clausthal-Zellerfeld, Germany*

Received 14 June 2006; received in revised form 20 August 2006; accepted 22 August 2006

Available online 6 October 2006

## Abstract

The electrochemical behaviour of Au(1 1 1) and highly oriented pyrolytic graphite (HOPG) substrates in the air- and water-stable ionic liquid 1-butyl-1-methylpyrrolidinium bis(trifluoromethylsulfonyl)amide ([BMP]Tf<sub>2</sub>N) was investigated using in situ scanning tunneling microscopy (STM). Furthermore, the electrodeposition of Se, In and Cu in the same ionic liquid was investigated. The high thermal stability as well as the large electrochemical window of this ionic liquid compared with aqueous electrolytes allow the direct electrodeposition of grey selenium, indium and copper at variable temperatures, as the first step in making CIS solar cells electrochemically, in a one pot reaction. The results show that grey selenium can be obtained at temperatures  $\geq 100^\circ\text{C}$ . XRD patterns of the electrodeposit obtained at  $100^\circ\text{C}$  show the characteristic peaks of crystalline grey selenium. Nanocrystalline indium with grain sizes between 100 and 200 nm was formed in the employed ionic liquid, containing 0.1 M InCl<sub>3</sub>, at room temperature. It was also found that copper(I) species can be introduced into the ionic liquid [BMP]Tf<sub>2</sub>N by anodic dissolution of a copper electrode and nanocrystalline copper with an average crystallite size of about 50 nm was obtained without additives in the resulting electrolyte.

© 2006 Elsevier Ltd. All rights reserved.

**Keywords:** Semiconductors; Electrodeposition; Ionic liquids; In situ STM; Selenium

## 1. Introduction

Selenium exhibits both photovoltaic action, where light is converted directly into electricity, and photoconductive properties, where the conductivity increases with increased illumination. These properties make selenium useful in the production of photocells and solar cells. Moreover, compound semiconductors containing selenium, such as InSe, CdSe or CuInSe<sub>2</sub> (CIS), have many optoelectric applications, including advanced solar cells, IR detectors and solid-state lasers [1].

The electrodeposition of selenium in aqueous solutions has been studied intensively, see for example [2–5]. However, the exclusive electrodeposition of grey selenium has not yet been successful in aqueous solutions. The electrodeposition of sele-

mium in aqueous solutions is usually complicated by the formation of amorphous red selenium, which exhibits bad electronic conductivity. Grey selenium can be deposited exclusively at elevated temperatures of more than  $100^\circ\text{C}$ , which is practically impossible to be achieved in aqueous galvanic baths. It is known that thermodynamically a phase transition from amorphous red to crystalline grey selenium occurs at a temperature of about  $100^\circ\text{C}$ . Therefore, the use of ionic liquids, especially the air- and water-stable ones, in the electrodeposition of selenium is of great benefit owing to their extraordinary physical properties. They exhibit good electrical conductivity, low vapour pressure, wide electrochemical windows and high thermal stability. For further information we would like to refer to a recent review from us [6]. Consequently, the direct electrodeposition of grey selenium and its compounds is possible in ionic liquids since the deposition process can be efficiently performed at elevated temperatures due to the very low vapour pressure of most of the liquids.

Copper and indium are regarded as important precursors for the production of compound semiconductors with selenium. The electrodeposition of copper in chloroaluminate ionic liq-

\* Corresponding author. Fax: +49 5323 722460.

E-mail address: [frank.endres@tu-clausthal.de](mailto:frank.endres@tu-clausthal.de) (F. Endres).

<sup>1</sup> Permanent address: Electrochemistry and Corrosion Laboratory, National Research Centre, Dokki, Cairo, Egypt.

<sup>2</sup> Permanent address: Inorganic Chemistry Department, National Research Centre, Dokki, Cairo, Egypt.

uids has been widely investigated [7–10]. It has been found that the reduction of  $\text{Cu}^{2+}$  to metallic Cu occurs in two one-electron steps: in the first step  $\text{Cu}^+$  is formed, in the second step the metal is deposited [7,8]. At high overvoltages for the deposition, alloying with Al sets in [9]. Using in situ STM, Endres and Schweizer [10] have shown that the bulk deposition of copper from acidic chloroaluminate liquids on Au(1 1 1) is preceded by three underpotential processes. Furthermore, the electrode potential for the redox process  $\text{Cu}^+/\text{Cu}^{2+}$  is more positive than the surface oxidation of Au(1 1 1) in that liquid. The electrodeposition of copper in basic chloroaluminate ionic liquids has also been reported [11]. As aluminium can only be deposited from the acidic liquids, the complexity of Cu–Al alloy formation can be avoided in basic liquids. The electrodeposition of Cu from a basic 1-ethyl-3-methylimidazolium tetrafluoroborate and a Lewis acidic  $\text{ZnCl}_2$ -1-ethyl-3-methylimidazolium chloride room temperature ionic liquid has been investigated [12,13]. Furthermore, the electrodeposition of Pd–In [14] and InSb [15] were investigated in ionic liquids.

In the first section of this paper, in situ STM results concerning the electrochemical behaviour of Au(1 1 1) and of HOPG substrates in the air- and water-stable ionic liquid 1-butyl-1-methylpyrrolidinium bis(trifluoromethylsulfonyl) amide ([BMP]Tf<sub>2</sub>N) are presented. This was to explore the influence of the ionic liquid on the substrates, to better understand the deposition processes in the employed ionic liquid. We have shown in a recent paper that the surface of Au(1 1 1) is subject to a restructuring/reconstruction in the ionic liquid [BMP]Tf<sub>2</sub>N [16]. As we know from Al deposition that pyrrolidinium cations in contrast to imidazolium cations lead to nanocrystalline deposits, it seemed of interest to shed further light on this subject, as we observe here, that the deposits are also nanocrystalline.

In the second part, results concerning the direct electrodeposition of crystalline grey selenium in 1-butyl-1-methylpyrrolidinium bis(trifluoromethylsulfonyl) amide ([BMP]Tf<sub>2</sub>N) containing  $\text{SeCl}_4$  at variable temperatures are reported. Furthermore, we present results on the electrodeposition of indium and copper in the same liquid, as possible first steps in the formation of InSe and  $\text{CuInSe}_2$  (CIS) semiconductor thin films.

## 2. Experimental

The ionic liquid 1-butyl-1-methylpyrrolidinium bis(trifluoromethylsulfonyl) amide ([BMP]Tf<sub>2</sub>N) was obtained from Merck KGaA (EMD) in the highest available quality. The liquid was dried under vacuum for 12 h at a temperature of 100 °C, to a water content below 3 ppm (by Karl–Fischer titration) and stored in an argon filled glove box, with water and oxygen levels below 1 ppm (OMNI-LAB from Vacuum-Atmospheres).  $\text{SeCl}_4$  (Alfa, 99.5%) and  $\text{InCl}_3$  (Alfa, 99.999%) were used without further purification.

All liquid preparations as well as the electrochemical measurements were performed in the glove box using a VersaStat<sup>TM</sup> II Potentiostat/Galvanostat (Princeton Applied Research) controlled by PowerCV and PowerStep software. Gold substrates from Arrandee (gold films of 200–300 nm thickness deposited on chromium-covered borosilicate glass), Au(1 1 1) (gold on

mica, purchased from Molecular Imaging), highly oriented pyrolytic graphite (HOPG), glassy carbon substrates (Alfa) and platinum sheets of thickness 0.5 mm (Alfa, 99.99%) were used as working electrodes, respectively. Directly before use, the gold substrates were very carefully heated in a hydrogen flame to red glow, HOPG substrates were freshly cleaved, Pt-substrates were cleaned for 10 min in an ultrasonic bath in acetone then heated in a hydrogen flame to red glow for a few minutes. Glassy carbon substrates were cleaned by refluxing in isopropanol followed by drying under vacuum. Pt-wires (Alfa, 99.99%) were used as quasi-reference and counter electrodes, respectively. Currently Pt-quasi reference electrodes are only a compromise as well defined reference electrodes in ionic liquids, especially for in situ STM, are still missing. A quartz round bottom flask was used as the electrochemical cell. Prior to use, all parts in contact with the solution were thoroughly cleaned in a mixture of 50/50 vol.%  $\text{H}_2\text{SO}_4/\text{H}_2\text{O}_2$  followed by refluxing in bidistilled water.

A high-resolution field emission scanning electron microscope (Carl Zeiss DSM 982 Gemini) was utilized to investigate the surface morphology of the deposited layers and energy dispersive X-ray analysis was used to determine the film composition. The X-ray diffractograms of the deposits were acquired by a Siemens D-5000 diffractometer with  $\text{Co K}\alpha$  radiation.

The STM experiments were performed using self-built STM heads and scanners under inert gas conditions ( $\text{H}_2\text{O}$  and  $\text{O}_2 < 1$  ppm) with a Molecular Imaging PicoScan 2500 STM controller in feedback mode. The STM experiments were performed in an air-conditioned laboratory with  $\Delta T < \pm 1$  °C. STM tips were prepared by electrochemical etching of platinum–iridium wires (0.25 mm diameter) and electrophoretically coated with an electropaint (BASF ZQ 84-3225 0201). During the STM experiments the electrode potential was controlled by the PicoStat from Molecular Imaging.

## 3. Results and discussions

### 3.1. In situ STM in [BMP]Tf<sub>2</sub>N

In order to get information on the effect of the ionic liquid 1-butyl-1-methylpyrrolidinium bis(trifluoromethylsulfonyl) amide ([BMP]Tf<sub>2</sub>N) at the electrode/electrolyte interface, in situ STM measurements were performed (also see [16]). Fig. 1 shows a set of STM images of Au(1 1 1) in the dry ionic liquid [BMP]Tf<sub>2</sub>N, at different electrode potentials. As seen in the STM image of Fig. 1a, at the open circuit potential (–0.4 V versus  $\text{Fc}/\text{Fc}^+$ ), the gold surface was fairly rough, and only the Au(1 1 1) steps can be identified clearly. Such behaviour can be subject to an adsorbed film at the electrode surface. By shifting the potential to –0.7 V (versus  $\text{Fc}/\text{Fc}^+$ ), the Au(1 1 1) underwent a restructuring, with the formation of vacancy islands over the active surface, Fig. 1b. These defects were monoatomically deep. When the potential is set to more negative values, these vacancy islands disappear more and more (Fig. 1c), and at –1.6 V versus  $\text{Fc}/\text{Fc}^+$  the typical Au(1 1 1) surface with terraces of 250 pm in height is obtained (Fig. 1d). Approaching the potential region

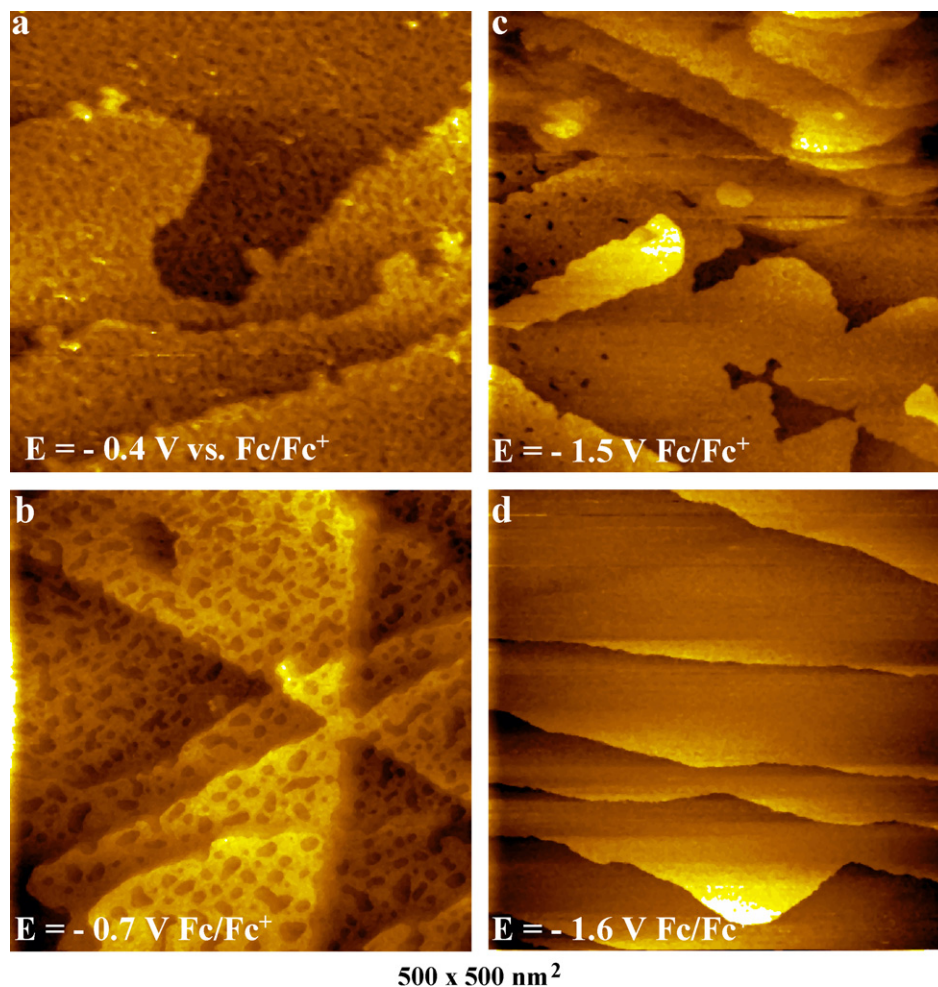


Fig. 1. STM pictures of Au(1 1 1) in the ionic liquid [BMP]Tf<sub>2</sub>N at different potentials.

where the bulk reduction of the ionic liquid occurs (at  $E = -2.8$  versus Fc/Fc<sup>+</sup>, see Ref. [16]), the surface roughness increases strongly and the gold terraces are completely concealed.

Based on these results, it was assumed that an adsorbed film induced the surface restructuring/reconstruction of the Au(1 1 1) on scanning the potential in the negative direction. Recent results in this laboratory made this assumption reasonable, as this surface reconstruction looks a bit different in the ionic liquid 1-ethyl-3-methylimidazolium bis(trifluoromethylsulfonyl) amide. Therefore, it was assumed that the [BMP]<sup>+</sup> cation was adsorbed at the electrode surface at potentials close to the open circuit potential. Neutralization of excess negative charge at the electrode surface by adsorbed cations might influence the Au–Au interaction facilitating gold atoms mobility on the surface, which, in turn, gave rise to the gold restructuring. In that context, it should be noted that [BMP]<sup>+</sup> appears to act as a grain refiner during electrodeposition of aluminium in the ionic liquid [BMP]Tf<sub>2</sub>N [17]. The aluminium deposit obtained in the ionic liquid [BMP]Tf<sub>2</sub>N was nanocrystalline with an average grain size around 30 nm, whereas in the ionic liquid [EMIm]Tf<sub>2</sub>N it was microcrystalline [17]. Presumably [BMP]<sup>+</sup> was adsorbed at the surface of growing nuclei, thus hindering the further growth of Al crystallites. This finding is in agreement with STM results

which indicate an adsorption, presumably [BMP]<sup>+</sup>, at the gold surface inducing a Au(1 1 1) surface restructuring. The determination of the potential of zero charge (pzc) might help to investigate the role of cations and/or anions on the behaviour of Au(1 1 1) in ionic liquids.

In order to shed light on this suggested surface film, investigations of the behaviour of highly oriented pyrolytic graphite (HOPG) in the ionic liquid [BMP]Tf<sub>2</sub>N, were carried out using in situ STM. HOPG is a well-defined surface, which is not subject to restructuring. Fig. 2 shows a sequence of STM images, obtained at different electrode potentials, before cathodic decomposition of the ionic liquid set in. It is worth noting that the quality of the STM images degraded at potentials close to open circuit potential. This image quality degradation (even in ultrapure [BMP]Tf<sub>2</sub>N) appeared systematic. The quality of the images improved on scanning the potential in the negative direction. Poor image quality could be attributable to some sort of adsorption at the electrode surface. The STM image obtained at  $-2.1$  V (versus Fc/Fc<sup>+</sup>), Fig. 2a, showed a more or less typical HOPG surface with flat steps height about two graphite monolayers. Shifting the potential to  $-2.5$  V (versus Fc/Fc<sup>+</sup>), an apparent etching of the step edges sets in as seen in the STM picture of Fig. 2b. In our opinion this observation

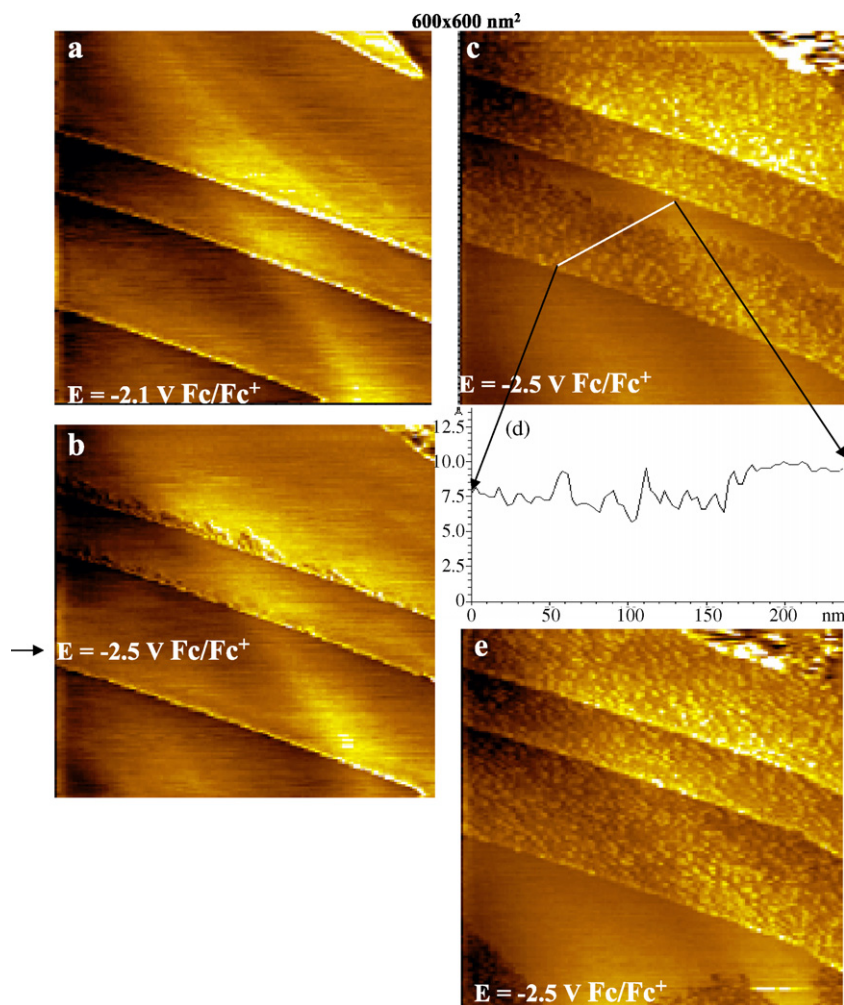


Fig. 2. STM pictures of HOPG in the ionic liquid [BMP]Tf<sub>2</sub>N at different potentials, a, b, c and e. (d) Height profile along the white line shown in the STM picture (c).

signifies the starting breakdown or the reductive desorption of the adsorbed film at the step edges. Breakdown/desorption continued at the flat terraces (Fig. 2c). A height profile (Fig. 2d) indicated the height of the adsorbed film was in the range of 200–300 pm. On further STM scanning at the same potential (prior to the massive reduction of the organic cation of the ionic liquid,  $-2.7$  V versus Fc/Fc<sup>+</sup>) [18], the surface roughness increased as a consequence of the reductive breakdown of the adsorbed film, Fig. 2e. We would like to mention that we have not yet succeeded in getting atomic resolution of HOPG in [BMP]Tf<sub>2</sub>N, maybe a result of the suggested surface film.

### 3.2. Electrodeposition in [BMP]Tf<sub>2</sub>N

Bearing in mind that the cation of [BMP]Tf<sub>2</sub>N seems to adsorb on electrode surfaces and growing nuclei, in the following section, results concerning the electrodeposition of grey selenium, indium and copper from the same ionic liquid were studied as a function of temperature. The high thermal stability of this ionic liquid (up to about 300 °C) allowed direct electrodeposition of grey selenium at elevated temperatures.

#### 3.2.1. Electrodeposition of selenium

The cyclic voltammograms of [BMP]Tf<sub>2</sub>N, containing 0.1 mol/L SeCl<sub>4</sub>, on a Pt substrate at different temperatures, are displayed in Fig. 3. The potential started at the open circuit potential and was initially swept in the negative direction at a scan rate of 10 mV/s. In these experiments we had no other choice but to employ a Pt quasi-reference. The peaks for Fc/Fc<sup>+</sup> were difficult to identify, and due to the complexity of the voltammograms, it was decided to avoid any interference from ferrocene. Fortunately, the Pt quasi-reference electrode was fairly stable in the course of the experiment. At 25 °C, the cyclic voltammogram was characterised by a main cathodic peak at  $-0.75$  V (versus Pt), c<sub>3</sub>, and two shoulders, c<sub>2</sub> and c<sub>1</sub>, preceding c<sub>3</sub>. As a dark red deposit was obtained at  $-0.75$  V after deposition for 2 h, the main reduction peak, c<sub>3</sub>, might be attributed to the reduction of Se(IV) to elemental Se, presumably the red phase, and the two shoulders c<sub>2</sub> and c<sub>1</sub> might be associated with two different under potential deposition processes. The anodic peak a<sub>3</sub> recorded in the reverse scan was ascribed to partial dissolution of the deposited selenium. The anodic counterparts to the cathodic peaks c<sub>1</sub> and c<sub>2</sub> (a<sub>1</sub> and a<sub>2</sub>) were recorded at potentials higher than 0.0 V. From the experiments at 25 °C it was con-

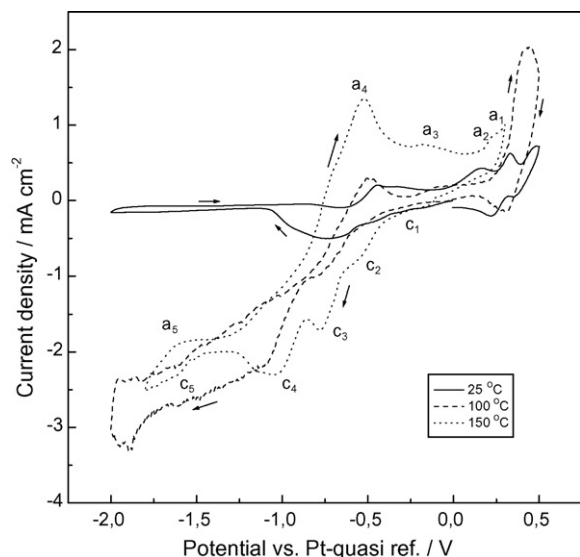


Fig. 3. Cyclic voltammograms of the ionic liquid 1-butyl-1-methyl pyrrolidinium bis(trifluoromethylsulfonyl)amide containing 0.1 M  $\text{SeCl}_4$  on platinum at different temperatures. Scan rate 10 mV/s.

cluded that a thin film of X-ray amorphous red selenium was obtained. This result is not at all surprising, given that thermodynamically a phase transition from amorphous red selenium to crystalline grey selenium occurs only at temperatures  $\geq 100^\circ\text{C}$ . Thus, the exclusive deposition of grey selenium should occur at temperatures above  $100^\circ\text{C}$ . Cyclic voltammetry measurements at 100 and  $150^\circ\text{C}$  were also performed, and are present as the dashed curves in Fig. 3. Two new cathodic processes were evident in the cathodic branch,  $c_4$  and  $c_5$ , with corresponding anodic counterparts,  $a_4$  and  $a_5$ , respectively. At  $c_3$ , a red deposit was evident on the electrode surface with the naked eye, which turned grey at  $c_4$ . Thus, the peaks  $c_3$  and  $c_4$  are likely related to deposition of red and grey selenium, respectively. When the potential was scanned further in the negative direction, after formation of the grey selenium deposit, a further cathodic peak  $c_5$  was observed, with corresponding anodic peak  $a_5$ . This pair of peaks might be associated with further reduction of the deposited selenium to  $\text{Se}^{2-}$  as the selenium film can disappear completely at this potential. It should be mentioned that the reduction of selenium to  $\text{Se}^{2-}$  has been reported in aqueous solutions [19–22]. Our results show that selenium electrochemistry in [BMP][Tf<sub>2</sub>N] ionic liquid is fairly difficult and requires a lot of fundamental studies.

In order to perform a material analysis of selenium, the deposits were made at  $-1.1\text{ V}$  (versus Pt) for 2 h at  $100^\circ\text{C}$  on Pt substrates and subsequently characterised by means of SEM-EDAX and XRD to explore morphology and composition. After the deposition experiments the deposits were washed by isopropanol and then cleaned with acetone in an ultrasonic bath for 10 min. Visually, a dark grey, well adherent deposit was obtained after potentiostatic deposition. As seen in the SEM micrograph shown in Fig. 4a, the deposit made at  $100^\circ\text{C}$  appeared dense with a flower-like structure. The EDX profile of Fig. 4c revealed only selenium in the deposit. There was neither chloride nor any component of the ionic liquid in the deposited film. The XRD

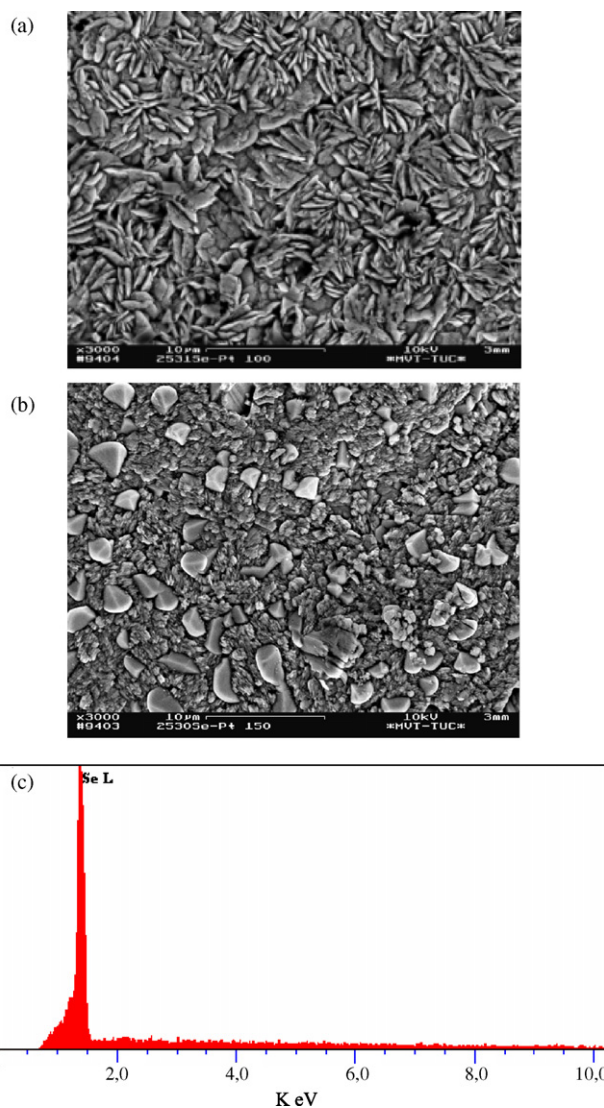


Fig. 4. SEM micrographs of electrodeposited Se layers obtained potentiostatically on Pt in the ionic liquid [BMP][Tf<sub>2</sub>N] containing 0.1 M  $\text{SeCl}_4$  at a potential of  $-1.1\text{ V}$  (vs. Pt) for 2 h at (a)  $100^\circ\text{C}$  and (b)  $150^\circ\text{C}$ . (c) EDAX profile of the area shown in the SEM micrograph (a).

patterns of the electrodeposit showed the characteristic peaks of the crystalline grey selenium, Fig. 5. At a deposition temperature of  $150^\circ\text{C}$  the morphology of the films changed slightly (Fig. 4b) but the XRD showed also only grey selenium. At this temperature red or black selenium would be thermodynamically excluded.

### 3.2.2. Electrodeposition of Indium

Fig. 6 shows the cyclic voltammogram of the ionic liquid [BMP][Tf<sub>2</sub>N] containing 0.1 M  $\text{InCl}_3$ , at a glassy carbon electrode, at  $25^\circ\text{C}$ . As seen, the cyclic voltammogram exhibits a rapid increase of the cathodic current at a potential of about  $-1.75\text{ V}$  (versus Pt) as a result of the bulk deposition of indium. This signifies that the reduction of  $\text{In}^{3+}$  to  $\text{In}^0$  occurs in one step. In the reverse scan, an anodic peak at  $-2.0\text{ V}$  suggests partial stripping of the electrodeposited indium. The increase in anodic current at about  $0.0\text{ V}$  might be the result of slower

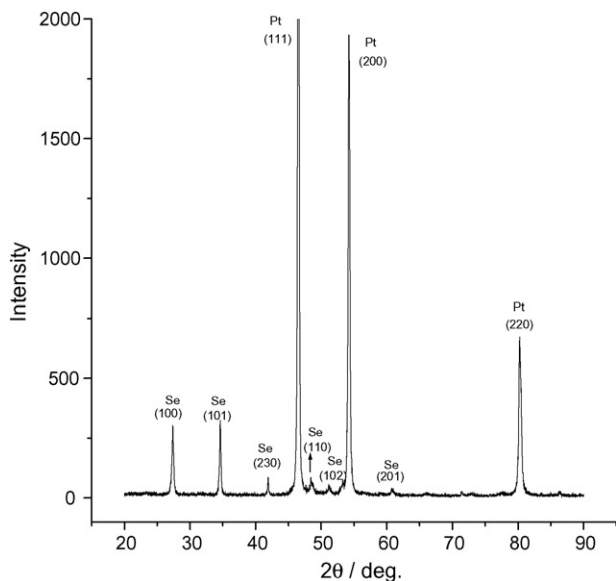


Fig. 5. XRD patterns of an electrodeposited Se layer obtained potentiostatically on Pt in [BMP]Tf<sub>2</sub>N containing 0.1 M SeCl<sub>4</sub> at a potential of  $-1.1$  V (vs. Pt) for 2 h at  $100^\circ\text{C}$ .

dissolution of larger In crystallites. After the cyclic voltammetry experiment, a metallic film of indium was clearly seen on the electrode surface indicating the incomplete stripping of the electrodeposited indium. As previously shown by this group, with tantalum deposition, reoxidation of the deposits seems to be hindered in [BMP]Tf<sub>2</sub>N [23].

The electrodeposition of indium on polycrystalline platinum substrates was also investigated in this electrolyte. The cyclic voltammograms recorded at Pt substrates with different reversal potentials are shown in Fig. 7. Unlike in the case of glassy carbon, several cathodic processes,  $c_1$ – $c_4$ , are recorded at platinum substrate, prior to bulk deposition of indium, Fig. 7a. Visually, bulk deposition was found to occur at  $c_5$ . As cathodic peaks  $c_1$ – $c_4$  occur at potentials positive to the potential of bulk deposition of In, they are presumably correlated with different UPD processes for In on polycrystalline platinum. In order to obtain

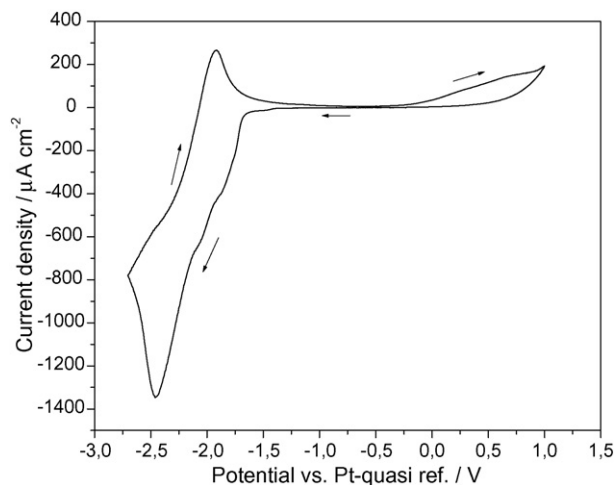


Fig. 6. Cyclic voltammogram of the ionic liquid [BMP]Tf<sub>2</sub>N containing 0.1 M InCl<sub>3</sub> on glassy carbon at  $25^\circ\text{C}$ . Scan rate 10 mV/s.

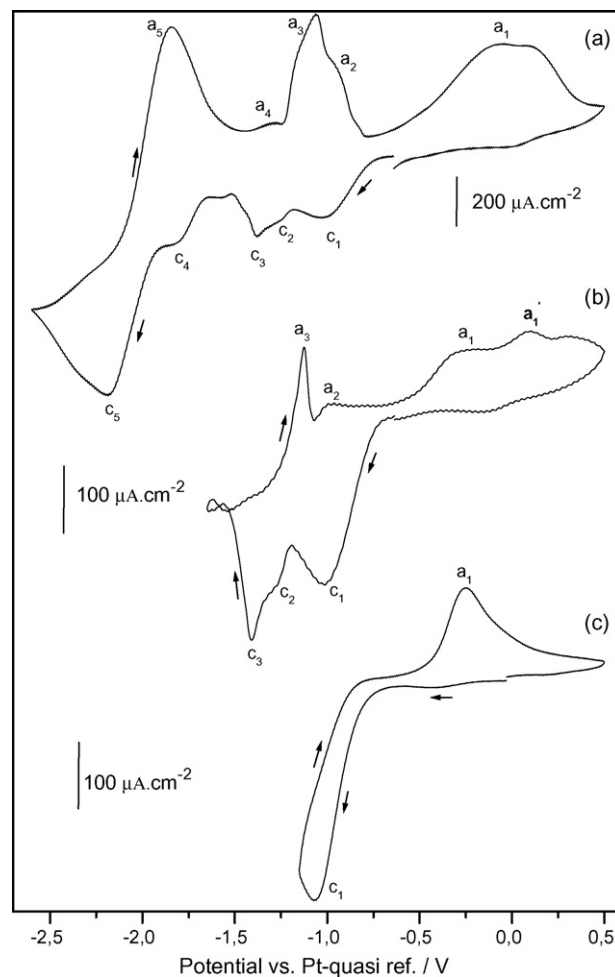


Fig. 7. Cyclic voltammograms of the ionic liquid [BMP]Tf<sub>2</sub>N containing 0.1 M InCl<sub>3</sub> on platinum with different reversal potentials at  $25^\circ\text{C}$ . Scan rate 10 mV/s.

more information on the different electrochemical processes, cyclic voltammograms with varying reversal potentials were performed, Fig. 7b and c. If the scan was reversed at a potential of  $-1.1$  V, only one reduction peak,  $c_1$ , was observed with the corresponding anodic peak,  $a_1$ , Fig. 7c. EDX analysis indicated a very low concentration of indium on the electrode after applying a constant potential of  $-1.1$  V for 1 h. The presence of indium at the electrode surface before bulk deposition suggests that this peak corresponds to a UPD process. At a lower switching potential  $-1.6$  V, two new cathodic peaks,  $c_2$  and  $c_3$ , were observed with corresponding anodic peaks,  $a_2$  and  $a_3$ , respectively (Fig. 7b). A further new anodic peak,  $a'_1$ , was observed at a potential more positive than the potential of the anodic peak  $a_1$ . This peak might result from alloying of In with Pt. As shown in Fig. 7a, a further new cathodic process ( $c_4$ ) with its counterpart ( $a_4$ ) was recorded prior to bulk deposition of In ( $c_5$ ). Those results showed that electrodeposition of indium on glassy carbon was relatively straightforward, whereas on platinum there was evidence for multiple UPD/alloying processes. This indicates a need to investigate In deposition on platinum using in situ scanning tunneling microscopy.

The surface morphology of In deposited on platinum in the ionic liquid [BMP]Tf<sub>2</sub>N, containing 0.1 M InCl<sub>3</sub>, after poten-

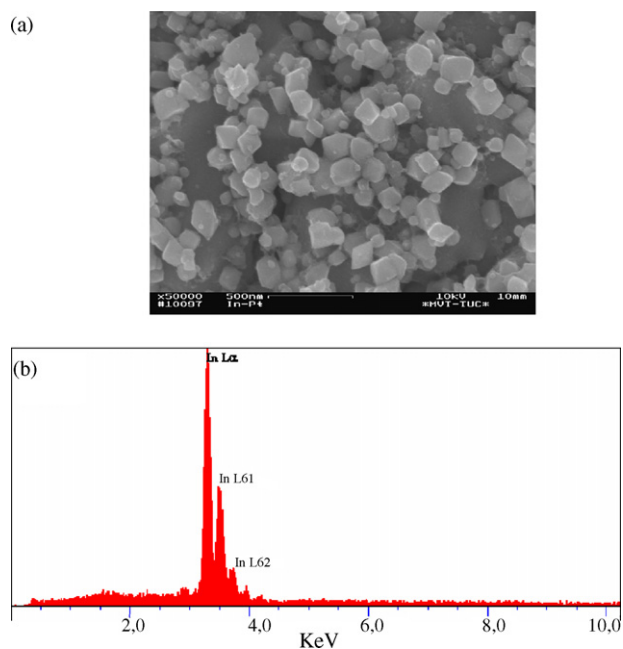


Fig. 8. (a) SEM micrograph of an electrodeposited indium film obtained potentiostatically on platinum in the ionic liquid [BMP]Tf<sub>2</sub>N containing 0.1 M InCl<sub>3</sub> at a potential of  $-2.2$  V (vs. Pt) for 2 h at 25 °C. (b) EDAX profile taken on a big crystallite.

tiostatic polarization at  $-2.2$  V (versus Pt) for 2 h is shown in Fig. 8a. The deposit consists of indium crystallites with sizes of approximately 100–200 nm. The accompanying EDX profile reveals the deposition of pure metallic indium, Fig. 8b.

The effect of increasing the temperature on the electrodeposition of indium on platinum substrates in the employed electrolyte was also investigated, Fig. 9. The cyclic voltammogram recorded at 50 °C exhibits the same general features of the cyclic voltammogram measured at 25 °C (see Fig. 7a). However, the cyclic voltammograms obtained at 100 and 150 °C

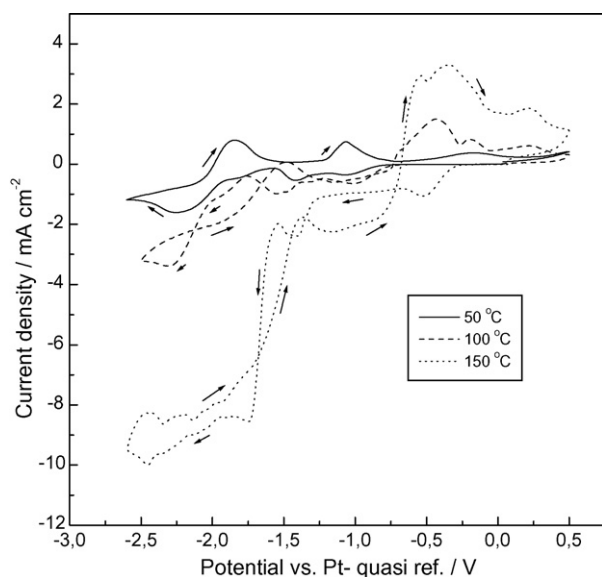


Fig. 9. Cyclic voltammograms of the ionic liquid [BMP]Tf<sub>2</sub>N containing 0.1 M InCl<sub>3</sub> on platinum at different temperatures. Scan rate 10 mV/s.

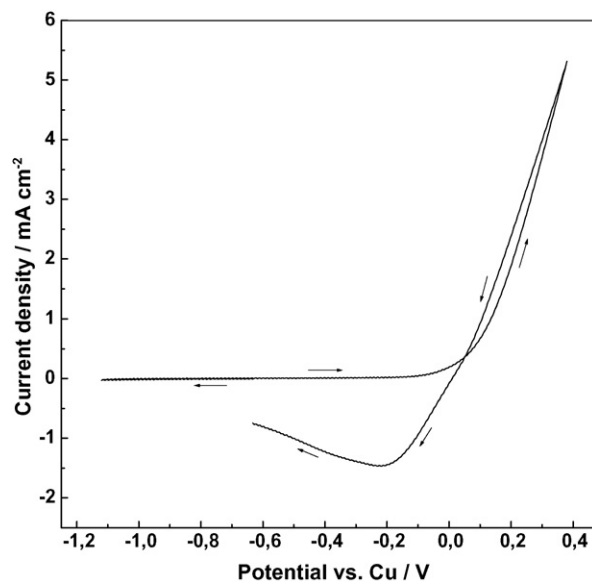


Fig. 10. Voltammetric behaviour of copper electrode in the ionic liquid [BMP]Tf<sub>2</sub>N. Scan rate 10 mV/s.

are significantly more complicated, and alloying with platinum seems to be facilitated. Moreover, the deposits obtained showed worse adherence. This was not surprising, as the melting point of indium is 156.6 °C and hence the deposition of adherent metallic indium might be difficult at temperatures close to its melting point. Nevertheless, these results show that indium can be electrodeposited in [BMP]Tf<sub>2</sub>N at temperatures above 100 °C, at temperatures where grey selenium can be obtained, as well.

### 3.2.3. Electrodeposition of copper

Copper can also be deposited from [BMP]Tf<sub>2</sub>N, at a variety of temperatures. Unfortunately, most copper compounds tested had only limited solubility in the ionic liquid [BMP]Tf<sub>2</sub>N, and the best method for introducing copper cations into the ionic liquid was anodic dissolution of a copper electrode. Fig. 10 shows the

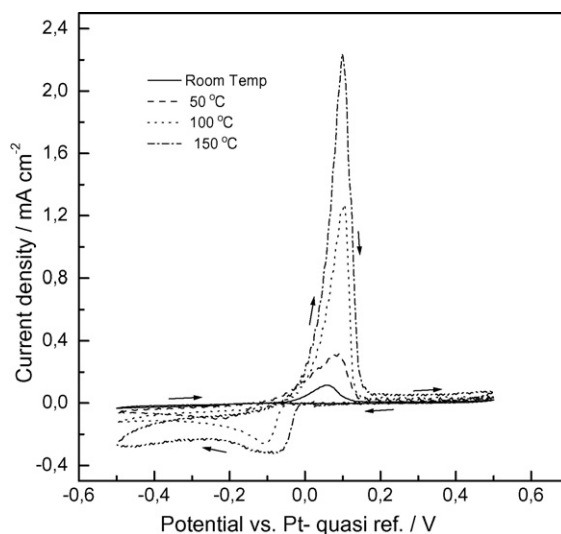


Fig. 11. Cyclic voltammograms of the ionic liquid [BMP]Tf<sub>2</sub>N containing 60 mmol/L Cu(I) on platinum at different temperatures. Scan rate 10 mV/s.

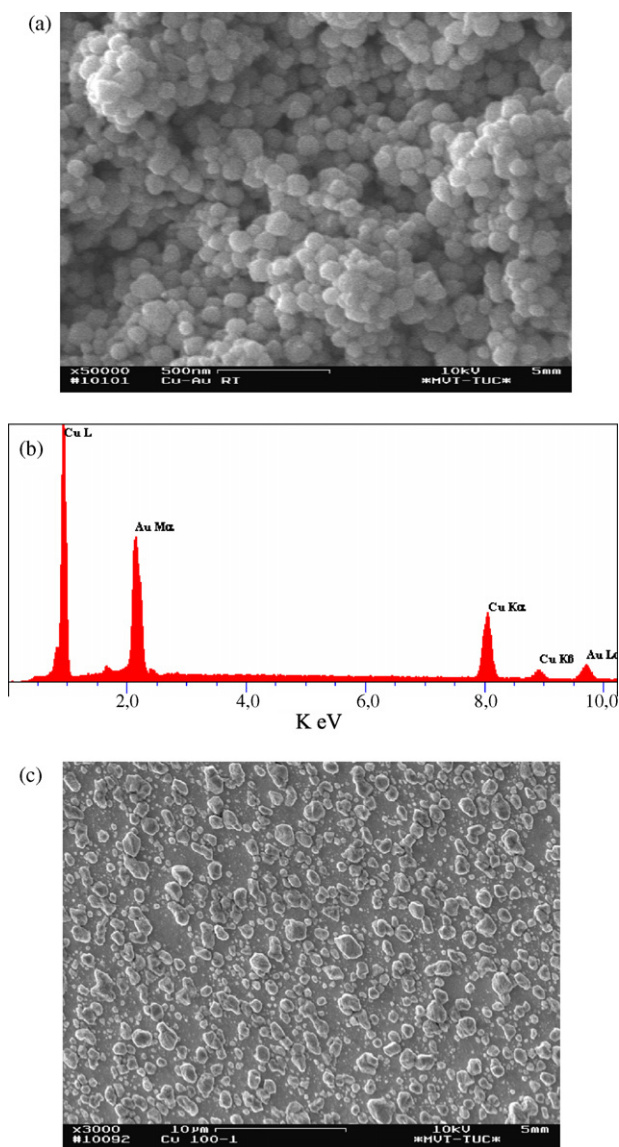


Fig. 12. (a) SEM micrograph of nanocrystalline copper obtained potentiostatically on Au in the ionic liquid [BMP]Tf<sub>2</sub>N containing 60 mmol/L Cu(I) at a potential of  $-0.25$  V (vs. Pt) for 2 h at room temperature. (b) EDAX profile of the area shown in the SEM micrograph. (c) SEM micrograph of a deposited Cu layer obtained potentiostatically at  $-0.12$  V (vs. Pt) for 2 h at  $100$  °C.

cyclic voltammogram of copper in the employed ionic liquid. The potential was scanned first in the negative direction down to  $-1.12$  V (versus Cu) then it was scanned back to  $+0.38$  V and finally stopped at the open circuit potential. It is clear that anodic dissolution of copper starts at a potential of  $+0.05$  V, indicated by the rapid increase in anodic current. The reduction peak observed at  $-0.2$  V (versus Cu) is attributed to redeposition of dissolved copper. Based on this information, Cu cations can be introduced into the ionic liquid by applying a positive potential,  $\geq +0.1$  V. In order to determine the oxidation state of the copper species, the weight loss of the copper electrode, as well as the charge consumed during its anodic dissolution at a potential of  $+0.3$  V (versus Cu) were measured. The oxidation state of copper species was found to be 1. This indicates that Cu(I), presumably Cu(Tf<sub>2</sub>N), was the product of the anodic dissolution of copper

electrode. It is unlikely that the Tf<sub>2</sub>N anion was decomposed at this electrode potential.

Fig. 11 presents cyclic voltammograms obtained for Cu(I) species on gold substrates at different temperatures, 25, 50, 100 and 150 °C. As shown, all cyclic voltammograms exhibit the same general features: there is a pronounced cathodic peak for copper deposition with its corresponding stripping peak. Increasing the temperature resulted in the deposition potential moving positive, as well as the current increasing. This was ascribed both to an increase in the mobility of the electroactive species towards the electrode surface and in a reduced nucleation overvoltage at elevated temperatures.

The SEM micrograph of Fig. 12a shows the surface morphology of an electrodeposited copper layer on gold substrate obtained at a constant potential of  $-0.250$  V (versus Pt) for 2 h in the ionic liquid [BMP]Tf<sub>2</sub>N containing 60 mmol/L of Cu(I) at 25 °C. As seen, the deposit is dense and contains fine crystallites with average sizes of about 50 nm. The deposit was analysed as metallic copper as revealed by the corresponding EDX profile, Fig. 12b. Interestingly, the deposited copper was nanocrystalline without any additive, similar to the deposition of nanocrystalline Al [17]. This finding is of some interest as nanocrystalline copper has excellent mechanical and electronic properties, superior to those of microcrystalline copper. The increase of temperature had a dramatic effect on the crystallite sizes as revealed in the SEM micrograph of Fig. 12c. The deposit made potentiostatically at  $-0.12$  V (versus Pt) for 2 h at 100 °C rather contained microcrystalline copper particles.

#### 4. Conclusions

In part 1 of the present paper, surface processes at the interface of Au(111) and HOPG in the ionic liquid 1-butyl-1-methylpyrrolidinium bis(trifluoromethylsulfonyl) amide ([BMP]Tf<sub>2</sub>N) were described. In situ STM showed that Au(111) was initially restructured to a worm-like surface, and to the typical Au(111) surface at more negative electrode potentials. On HOPG, a surface film, which disappeared at electrode potentials close to the cathodic decomposition of the liquid, was observed. Presumably, the cation of the ionic liquid was adsorbed, causing the restructuring/reconstruction of the Au(111) surface.

In part 2 the electrodeposition of grey selenium, indium and copper in [BMP]Tf<sub>2</sub>N at variable temperatures was described. A key result was that at temperatures above 100 °C, grey selenium was deposited as a single phase, whereas at 25 °C the red amorphous phase was formed. Both indium and copper were electrodeposited from [BMP]Tf<sub>2</sub>N at variable temperatures. Interestingly, the grain sizes of electrochemically formed In and Cu were in the nanosize regime. Based on former studies on the electrodeposition of aluminium, and based on in situ STM results both on Au(111) and on HOPG, it could be concluded that the [BMP]<sup>+</sup> cation was adsorbed on the substrates and on growing nuclei, leading to nanosized deposits. It is unclear at the moment to which extent the Tf<sub>2</sub>N anion is co-adsorbed. The possibility of depositing grey selenium, indium and copper in one ionic liquid, at variable temperatures, suggests that semicon-

ductor CuInSe<sub>2</sub> (CIS) might be formed electrochemically using such an ionic liquid.

## References

- [1] H.W. Schock, *Appl. Surf. Sci.* 92 (1996) 606.
- [2] B.M. Huang, T.E. Lister, J.L. Stickney, *Surf. Sci.* 392 (1997) 27.
- [3] T.A. Sorenson, T.E. Lister, B.M. Huang, J.L. Stickney, *J. Electrochem. Soc.* 146 (1999) 1019.
- [4] M. Alanyalioglu, U. Demir, C. Shannon, *J. Electroanal. Chem.* 561 (2004) 21.
- [5] X.Y. Zhang, Y. Cai, J.Y. Miao, K.Y. Ng, Y.F. Chan, X.X. Zhang, N. Wang, *J. Cryst. Growth* 276 (2005) 674.
- [6] F. Endres, S. Zein El Abedin, *Phys. Chem. Chem. Phys.* 8 (2006) 2101.
- [7] C.L. Hussey, L.A. King, R.A. Carpio, *J. Electrochem. Soc.* 126 (1979) 1029.
- [8] C. Nanjundiah, R.A. Osteryoung, *J. Electrochem. Soc.* 130 (1983) 1312.
- [9] B.J. Tierney, W.R. Pitner, J.A. Mitchell, C.L. Hussey, *J. Electrochem. Soc.* 145 (1998) 3110.
- [10] F. Endres, A. Schweizer, *Phys. Chem. Chem. Phys.* 2 (2000) 5455.
- [11] J.-J. Lee, B. Miller, X. Shi, R. Kalish, K.A. Wheeler, *J. Electrochem. Soc.* 148 (2001) C183.
- [12] P.-Y. Chen, I.-W. Sun, *Electrochim. Acta* 45 (1999) 441.
- [13] P.-Y. Chen, M.-C. Lin, I.-W. Sun, *J. Electrochem. Soc.* 147 (2000) 3350.
- [14] S.-I. Hsiu, C.-C. Tai, I.-W. Sun, *Electrochim. Acta* 51 (2006) 2607.
- [15] M.-H. Yang, M.-C. Yang, I.-W. Sun, *J. Electrochem. Soc.* 150 (2003) C544.
- [16] N. Borisenko, S. Zein El Abedin, F. Endres, *J. Phys. Chem. B* 110 (2006) 6250.
- [17] S. Zein El Abedin, E. Moustafa, R. Hempelmann, H. Natter, F. Endres, *Chem. Phys. Chem.* 7 (2006) 1535.
- [18] S. Zein El Abedin, N. Borisenko, F. Endres, *Electrochem. Commun.* 6 (2004) 510.
- [19] M.C. Santos, S.A.S. Machado, *J. Electroanal. Chem.* 567 (2004) 203.
- [20] N. Furuya, S. Motoo, *J. Electroanal. Chem.* 98 (1979) 189.
- [21] R. Modolo, M. Traore, O. Vittori, *Electrochim. Acta* 31 (1986) 859.
- [22] T.E. Lister, J.L. Stickney, *J. Phys. Chem.* 100 (1996) 19568.
- [23] S. Zein El Abedin, H.K. Farag, E.M. Moustafa, U. Welz-Biermann, F. Endres, *Phys. Chem. Chem. Phys.* 7 (2005) 2333.